Received: 25 July 2020 | Revised: 16 September 2020 | Accepted: 4 October 2020

DOI: 10.1002/eom2.12061

RESEARCH ARTICLE

EcoMat FUNCTIONAL MATERIALS FOR GREEN ENERGY AND ENVIRONMENT WILEY

Reducing V_{OC} loss via structure compatible and high lowest unoccupied molecular orbital nonfullerene acceptors for over 17%-efficiency ternary organic photovoltaics

Cenqi Yan[1] | Ruijie Ma[2] | Guilong Cai[3] | Tao Liu[2] | Jingshuai Zhu[4] | Jiayu Wang[4] | Yuhao Li[3] | Jiaming Huang[1] | Zhenghui Luo[2] | Yiqun Xiao[3] | Xinhui Lu[3] | Tao Yang[5] | Xiaowei Zhan[4] | He Yan[2] | Gang Li[1]

[1]Department of Electronic and Information Engineering, The Hong Kong Polytechnic University, Hong Kong, China

[2]Department of Chemistry and Hong Kong Branch of Chinese National Engineering Research Center for Tissue Restoration & Reconstruction, Hong Kong University of Science and Technology (HKUST), Hong Kong, China

[3]Department of Physics, Chinese University of Hong Kong, Hong Kong, China

[4]Department of Materials Science and Engineering, College of Engineering, Key Laboratory of Polymer Chemistry and Physics of Ministry of Education, Peking University, Beijing, China

[5]College of New Materials and New Energies, Shenzhen Technology University, Shenzhen, China

Correspondence
Gang Li, Department of Electronic and Information Engineering, The Hong Kong Polytechnic University, Hong Kong 999077, China.
Email: gang.w.li@polyu.edu.hk

Tao Liu and He Yan, Department of Chemistry and Hong Kong Branch of Chinese National Engineering Research Center for Tissue Restoration & Reconstruction, Hong Kong University of Science and Technology (HKUST), Hong Kong 999077, China.
Email: liutaozhx@ust.hk (T. L.), hyan@ust.hk (H. Y.)

Funding information
the Hong Kong Polytechnic University, Grant/Award Numbers: 1-ZE29, Work Programme: YW3Y; the National Key Research and Development Program of China, Grant/Award Number: 2019YFA0705900; Hong Kong Innovation and Technology Commission, Grant/Award Numbers: ITC-CNERC14SC01, ITS/471/18; Hong Kong PhD Fellowship

Abstract

The ternary strategy is effectual to attain high-performance organic photovoltaics (OPVs). Herein, device processing and performance of PM6:Y6:IT-4F OPVs is improved, and ITIC-Th with high-lying lowest unoccupied molecular orbital is incorporated into PM6: Y6 blend. The PM6:Y6: ITIC-Th device afforded an excellent PCE of 17.2%, surpassing PM6: Y6 device, and becoming one of the highest PCE. The resulting ITIC-Th-based ternary OSCs demonstrated low energy loss (E_{loss}) of 0.53 to 0.54 eV, as compared to their binary counterparts with either high open-circuit voltage (V_{OC}) but large E_{loss}, or less E_{loss} but low V_{OC}. The incorporation of ITIC-Th and IT-4F balanced the charge mobilities, and thereby retained and improved fill factors. Increased crystalline coherence length and smaller d-spacing of π-π peaks are also observed in ternary blends, indicating enhanced crystallinity and thus improved active-layer morphology. These findings demonstrate the feasibility of exploring the exciting pool of nonfullerene acceptors to pursue new breakthroughs of OPVs.

KEYWORDS

energy loss, morphology, nonfullerene acceptor, organic photovoltaics, ternary

Tao Liu and He Yan are co-corresponding authors

Scheme, Grant/Award Number: PF17-03929; National Natural Science Foundation of China, Grant/Award Numbers: 2019B030302007, 51961165102; the Research Grants Council of Hong Kong, Grant/Award Numbers: 14314216, 15218517, C5037-18G; Sir Sze-yuen Chung Endowed Professorship; the Basic and Applied Basic Research Major Program of Guangdong Province; the Hong Kong Research Grants Council, Grant/Award Numbers: R6021-18, 16303917, 16305915, 16322416, 606012; the Shen Zhen Technology and Innovation Commission, Grant/Award Numbers: JCYJ20170413154602102, JCYJ20170413173814007, JCYJ20170818113905024

1 | INTRODUCTION

Solar cells are a promising solution that harvests clean and renewable energy from the sun to address the challenges posed by energy crisis and environmental contamination. Solution-processed bulk-heterojunction (BHJ) organic photovoltaics (OPVs) have risen as a promising competitor of silicon-based solar cells due to benefits of abundant raw materials, eco-friendliness, low production cost, excellent low-light performance, low-temperature processing, and easy fabrication into mechanically flexible, lightweight, and semitransparent devices. OPVs are therefore promising for versatile terrestrial and outer space applications.[1-11] Currently, nonfullerene acceptors, especially fused-ring electron acceptors (FREAs), are a research hotspot of BHJ OPVs, setting new records of power conversion efficiencies (PCEs).[12-20] Unlike fullerene derivatives (eg, $PC_{61}BM$ and $PC_{71}BM$), FREAs offer the advantages of low cost, flexible adjustment of optoelectronic properties, strong absorption in the visible and near-infrared region.

Active-layer morphology has a close relationship with exciton dissociation, charge transport, and charge collection, and thus strongly influences the performance of OPVs.[21] Historically, optimizing active-layer morphology is as vital as the design of photoactive materials and interfacial materials. Several device engineering techniques have been reported to modulate morphology, such as thermal annealing, solvent vapor annealing, and solvent additives. However, the BHJ morphology, including the aspects of phase separation, molecular packing, crystallinity, and domain size, is very often sensitive to the previous strategies. In particular, in high-efficiency binary OPV systems, the technique of delicately tuning the active-layer morphology requires further study toward higher device performance.

The ternary blend strategy can effectively improve the performance of binary-blend OPVs, including efficiency and stability, without involving complicated tandem or multi-junction structures.[22,23] The third component in ternary OPVs can exert one or multiple benefits, including broadening/strengthening absorption spectra, facilitating charge generation/transfer/transport/collection, reducing carrier recombination, and optimizing/freezing the active-layer morphology.[24-30] For instance, Yan and coworkers incorporated IXIC-4Cl with an absorption edge of 1000 nm into PM7:ITC-2Cl binary system, to broaden the absorption of active layer. In another case, Zhan and coworkers incorporated 4,4′-Biphenol (BPO) into F-containing donor/fullerene blend. The hydrogen bond formed between F-containing donor and BPO forms the dense donor network, and freezes the film morphology, and thus improves the thermal stability of OSCs based on F-containing donors. Recently, Yang and coworkers reported the ternary blend of PTB7-Th/$PC_{71}BM$/IDIC with a more controlled structure via sequential solution deposition. IDIC near the cathode can improve the electron extraction and block holes to cathodes, delivering 14% to 21% PCE improvement to those conventional ternary blends. The utilization of the third component of a chemical structure assembling the host materials is also feasible to regulate morphology. Early in 2015, by comparing successful and failed multiple-donor systems, we found it was the harmonious co-existence of two structural compatible PTB7 and PBDTT-SeDPP that endowed the PTB7:PBDTT-SeDPP:$PC_{71}BM$ based ternary OPVs with an improved PCE of 8.7%.[28] FREAs generally present good planarity, when bulky side chains are not incorporated. Hence, the demand for structure compatibility can be easily meet in dual-FREAs based OPVs. Previously, we designed a near-infrared absorbing FREA (IHIC), which features

thienothiophene based fused hexacylic donor core, and exhibits an open-circuit voltage (V_{OC}) of 0.752 V and a PCE of 10.6% along with PTB7-Th.[31] Inspired by the success of PTB7:PBDTT-SeDPP:$PC_{71}BM$ ternary OPVs, we designed, synthesized, incorporated IHIC-N into PTB7-Th: IHIC binary system, which has naphthalene based fused-hexacylic donor core, assembles IHIC and guarantees the structure compatibility of IHIC-N and IHIC.[32] Moreover, IHIC-N has a 0.13-eV higher lowest unoccupied molecular orbital (LUMO) energy level than IHIC, which potentially improves $V_{OC.}$ PTB7-Th:IHIC: IHIC-N based ternary devices successfully delivered a higher PCE of 11.9% and an improved V_{OC} of 0.785 V in relative to the PTB7-Th: IHIC control group. The utilization of polymeric donors with deep HOMO as third component can improve V_{OC} and efficiency.[33,34] Our very recent work demonstrates the 5% incorporation of wide-bandgap polymer donor (PBT[E]BTz) with a deeper HOMO level than host PM6 can improve PCE from 15.43% to 16.26%.[35]

Early in 2017, Zou group reported the first A-DA'D-A pentacylic NFA (BZIC), which obtained a efficiency of 6.3% along with polymeric donor HFQx-T.[36] The A-DA'D-A type molecules have advantages over the A-D-A molecules.[37-40] First, the electron-deficient unit in the fused -ring core can increase D-A interactions, and enhance intermolecular and intramolecular interactions, which improves molecular aggregation and charge transport. Second, the strongly electron-donating pyrrole unit can elevate the HOMO level and reduce the Eg of the acceptors. Third, the alkyl chains attached to the nitrogen atoms of pyrrole can introduce steric hindrance and prevent excessive aggregation. On the basis of BZIC, Zou group recently designed another A-DA'D-A structure NFA (Y6), which achieved a very high PCE of 15.7% in both conventional and inverted device structures when blended with the polymeric donor PM6.[41,42] OSCs based on PM6: Y6 exhibited high electroluminescence quantum efficiency and low nonradiative recombination loss. Hence, Y6 and its derivatives are extensively reported and used in recent research work.[43-58] For instance, other D-A copolymer donors, such as PTQ10, P2F-EHP, D16, W1, and D18, have been paired with Y6 to achieve excellent PCEs of 15% to 18%.[59-63] Besides, several research groups employed fullerene derivatives and Y6 to construct dual-acceptors ternary OPVs. Hou and coworkers found that the loading of $PC_{61}BM$ into PM6: Y6 blend not only enhanced electron mobility but also increased the electroluminescence quantum efficiency, which simultaneously balanced charge transport and reduced nonradiative energy loss (E_{loss}). Consequently, the addition of $PC_{61}BM$ into PM6: Y6 improved the PCE from 15.3% to 16.2%, attributed to the simultaneous enhancement of V_{OC}, short-circuit current density (J_{SC}), and fill factor (FF). Parallelly, the PM6:Y6: $PC_{71}BM$ based device was demonstrated with PCEs of 16.67% for rigid-substrate devices and 14.06% for flexible ITO-free devices.[64] FREAs are also incorporated as the third component. As an example, Zhang and coworkers successfully achieved a 16.27% efficiency in ternary OPVs with PM6:Y6: IT-4F blend containing 20% IT-4F, which is structurally compatible with Y6, and simultaneously enhanced J_{SC} of 25.40 mA cm^{-2}, V_{OC} of 0.84 V and FF of 75.9%[65] were achieved. However, carbon disulfide (CS_2) vapor of about 40 seconds in the active layer treatment process is difficult to control. CS_2 is an enzyme inhibitor with cytotoxic effects that can disrupt the normal metabolism of cells, interfere with lipoprotein metabolism and cause vascular disease, neuropathy, and damage to organs. Besides, CS_2 is inflammable with a very low flashing point of −30°C and a low boiling point of 46.5°C, and the upper limit of exposure to CS_2 in the air of the workshop is only 20 ppm. Accordingly, CS_2 vapor treatment prohibits the ambient fabrication of OPVs for future commercialization. Moreover, the chosen third component (IT-4F) is a narrow-bandgap acceptor with low-lying LUMO, and thus more obvious V_{OC} improvement is expected along with NFAs of high-lying LUMO. Herein, we not only improved the device processing of PM6:Y6: IT-4F[66] based OPVs by using nonflammable chloroform solvent, but also designed the fascinating PM6:Y6: ITIC-Th[67] ternary blend, due to ITIC-Th's high LUMO of −3.93 eV. Relative to the PM6: Y6 control with a 16.7% efficiency, with a V_{OC} of 0.84 V, a J_{SC} of 25.5 mA cm^{-2} and a FF of 77.4%. The PM6:Y6: ITIC-Th ternary OPVs realized a higher PCE of 17.2% as a result of simultaneous improvement of V_{OC} (0.86 V), FF (78.2%), and J_{SC} (25.6 mA cm^{-2}). ITIC-Th is found to increase and balance the charge mobilities. Increased crystalline coherence length and smaller d-spacing of π-π peaks are observed with the third component incorporation, indicating enhanced crystallinity and thus improved morphology of the blend. To the best of our knowledge, 17.2% is one of the highest PCEs for OPVs. The dual-acceptor ternary OPV device shows clearly smaller E_{loss} than both binary OPV systems. These results delineate the feasibility of constructing dual-NFA based OPVs to fulfill the potential of the exciting pool of OPV materials reported.

2 | RESULTS AND DISCUSSION

Scheme 1A,B displays the chemical structures and the energy levels of PM6, ITIC-Th, and IT-4F and Y6. PM6 exhibits a highest occupied molecular orbital (HOMO) of

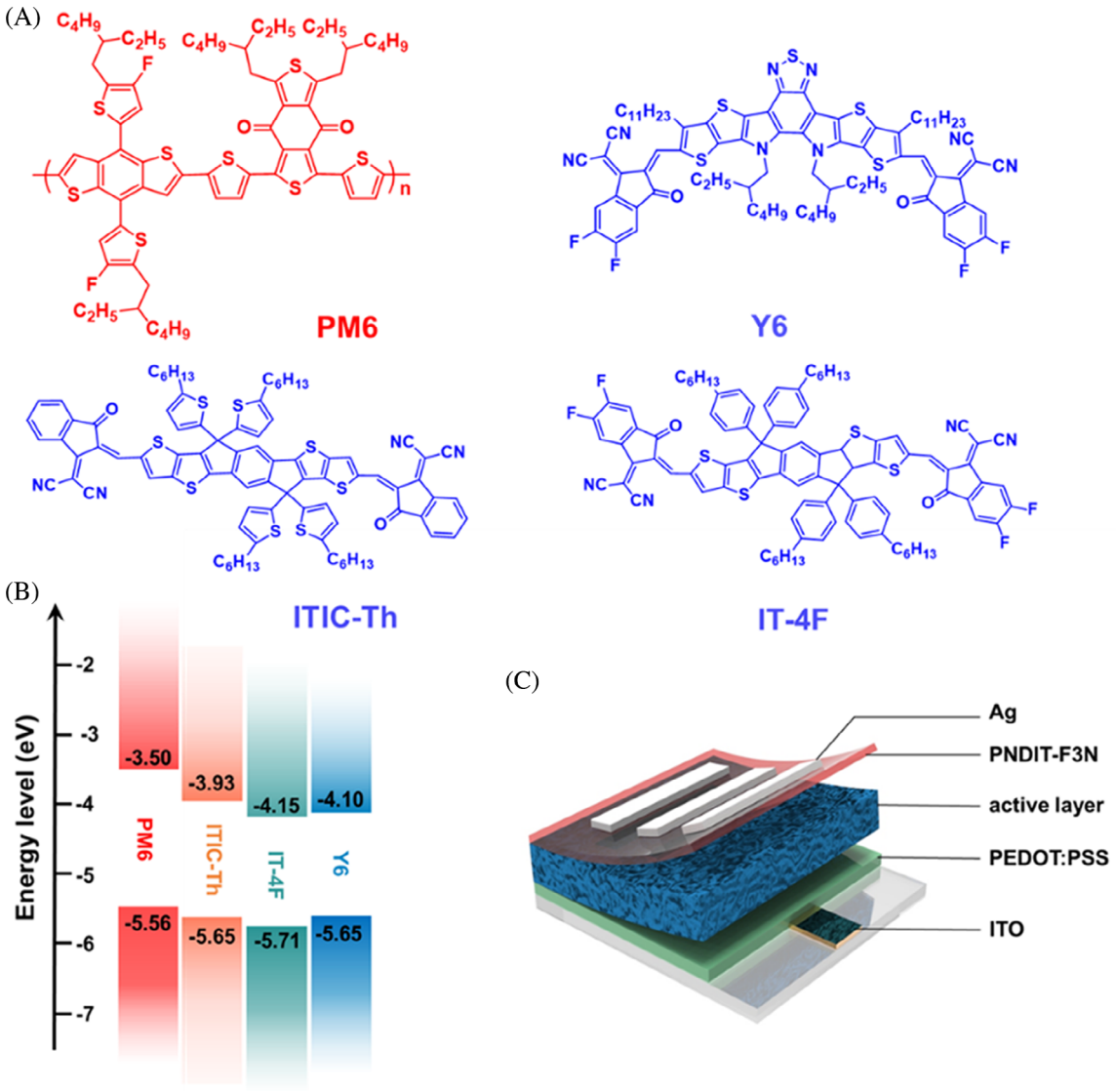

SCHEME 1 A, The chemical structures of PM6, Y6, IT-4F, and ITIC-Th; B, Energy level diagrams of all the active-layer materials; and C, The conventional device structure of ITO/ PEDOT: PSS/active layer/ PNDIT-F3N/Ag

−3.50 eV and a LUMO of −5.56 eV.[38] The energy levels of PM6: ITIC-Th, PM6: IT-4F, and PM6: Y6 systems are well aligned to split photo-generated excitons. The HOMO and LUMO of ITIC-Th are situated between those of PM6 and Y6, while IT-4F exhibits the lowest HOMO and LUMO. As shown in Figure 1A, PM6 displays an absorption onset of 668 nm; by comparison, ITIC-Th, IT-4F, and Y6 exhibit much red-shifted absorption onsets of 765, 804, and 925 nm. The optical bandgaps (E_g) are estimated by the intersections between the absorption and emission (Figure S1), and the bandgaps of ITIC-Th, IT-4F, and Y6 are calculated to be 1.67, 1.60, and 1.40 eV, respectively. A set of OPVs are fabricated based on PM6: Y6, PM6: IT-4F, PM6: Y6: IT-4F, PM6: ITIC-Th, and PM6: Y6: ITIC-Th systems, with the conventional device architecture of ITO/poly(3,4-ethylene dioxythiophene): poly(styrene sulfonate)(PEDOT: PSS)/ active layer/PNDIT-F3N/Ag (Scheme 1C).[68] These OPVs are fabricated using the same process parameters for direct comparison, which is summarized in Supporting Information.

Table 1 summarizes the best and average device characteristics based on PM6: acceptors (1:1.2 w/w) blended films. The current density-voltage (*J-V*) curves of the best devices under the illumination of an AM 1.5G solar simulator, 100 mW cm^{-2} are shown in Figure 1D,E. Among all the binary devices, the PM6: Y6 blend shows the highest PCE_{max} of 16.7%, the lowest V_{OC} of 0.84 V, the highest J_{SC} of 25.5 mA cm^{-2}, and the highest FF of 77.4%, along with E_{loss} of 0.56 eV. (E_{loss} can be calculated from the equation of $E_{loss} = E_g$-e$V_{OC,}$ where E_g is calculated from the crosspoint of the photoluminescence

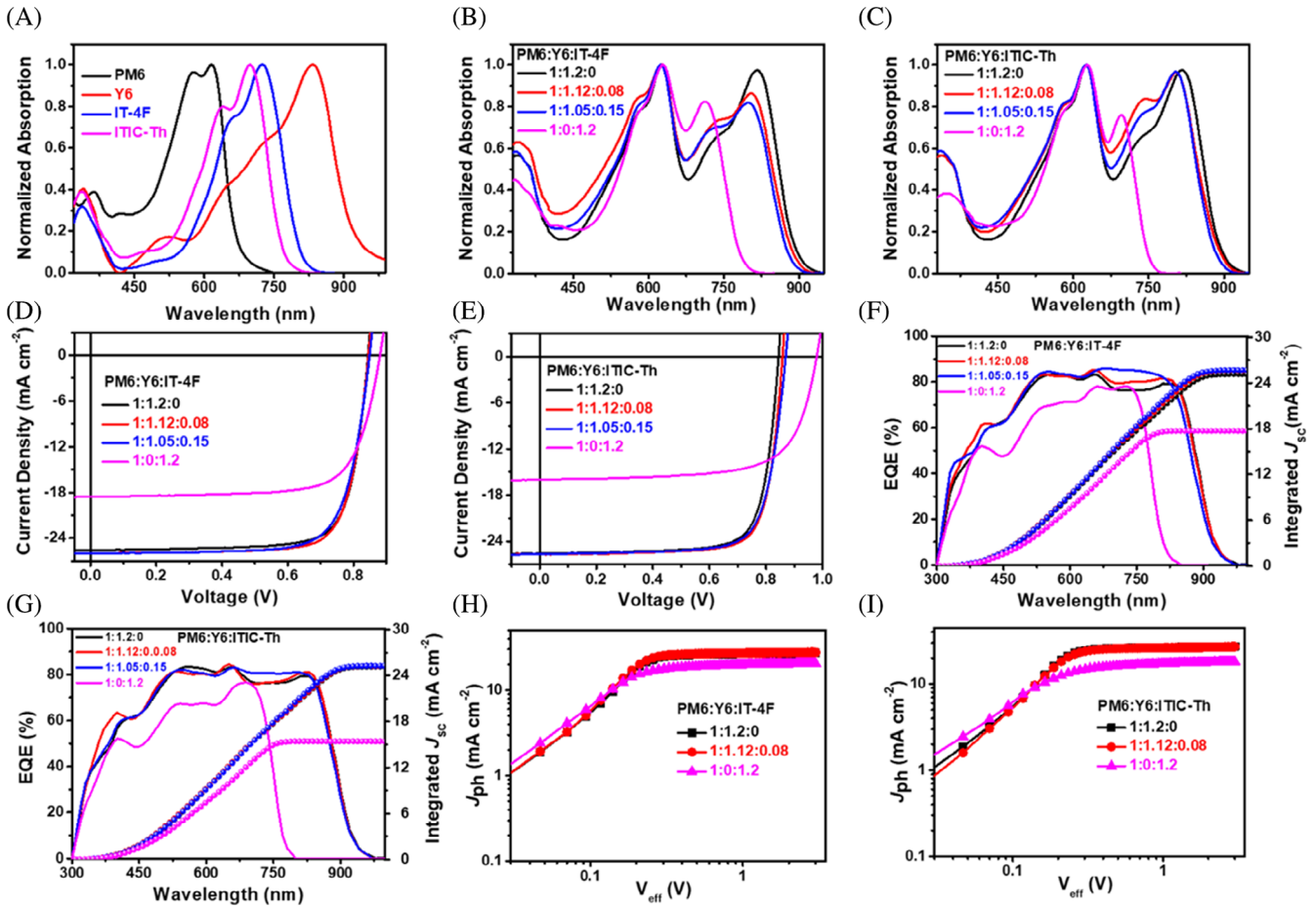

FIGURE 1 A, Normalized UV-vis absorption of PM6, Y6, IT-4F, and ITIC-Th pristine films; B, Normalized UV–vis absorption of PM6: Y6, PM6: Y6: IT-4F, and PM6: IT-4F blend films; C, Normalized UV–vis absorption of PM6: Y6, PM6: Y6: ITIC-Th, and PM6: ITIC-Th blend films; D, Current density-voltage (*J-V*) curves of OPVs based on PM6: Y6, PM6:Y6: IT-4F, and PM6: IT-4F blend films; E, Current *J-V* curves of OPVs based on PM6: Y6, PM6:Y6: ITIC-Th, and PM6: ITIC-Th blend films; F, External quantum efficiency (EQE) of OPVs based on PM6: Y6, PM6:Y6: IT-4F, PM6: IT-4F blend films; G, External quantum efficiency (EQE) of OPVs based on PM6: Y6, PM6:Y6: ITIC-Th, and PM6: ITIC-Th blend films; H, J_{ph} vs V_{eff} of OPVs based on PM6: Y6, PM6: Y6: IT-4F, and PM6: IT-4F blend films; and I, J_{ph} vs V_{eff} of OPVs based on PM6: Y6, PM6:Y6: ITIC-Th, and PM6: ITIC-Th blend films

[PL] and absorption spectra as shown in Figure S1) Such a high J_{SC} is ascribed to the wide and low-energy absorption at approximately 320 to 1100 nm of Y6. The PM6: IT-4F device exhibited a moderate PCE of 12.0%, with a V_{OC} of 0.88 V, a J_{SC} of 18.6 mA cm^{-2}, a FF of 73.3%, and E_{loss} of 0.72 eV. ITIC-Th exhibited more high-lying LUMO than IT-4F and Y6, and OPVs based on PM6: ITIC-Th exhibited a higher V_{OC} of 0.98 V and a higher E_{loss} of 0.69 eV than those of PM6:Y6. Nonetheless, this device only gave undesirable J_{SC} of 16.0 mA cm^{-2} and FF of 69.5%, leading to the lowest PCE of 10.9%. Hence, the success of the Y6 molecule is indeed attributed to the optimization of the trade-off between V_{OC} and J_{SC}.

Device data of ternary OPVs based on PM6: Y6: IT-4F and PM6: Y6: ITIC-Th (the weight ratio of D:A is 1:1.2) are also summarized in Table 1, and shown in Figure 1D, E. The PM6:Y6: IT-4F ternary devices achieved the optimal PCE of 17.0% at the weight ratio of 1:1.12:0.08, ascribed to the slightly increased V_{OC} of 0.85 V and J_{SC} of 26.0 mA cm^{-2}. As a comparison, the 6.7% loading of ITIC-Th simultaneously improved V_{OC} from 0.84 to 0.86 V, J_{SC} from 25.5 to 25.6 mA cm^{-2}, and FF from 77.4% to 78.2%, which synergistically contributes to its high PCE of 17.2%, which is one of the highest PCE for OPVs. The more obvious V_{OC} enhancement is attributed to the 0.22 eV higher LUMO of ITIC-Th than IT-4F. The PM6: Y6: ITIC-Th based OSCs presents E_{loss} of 0.53 to 0.54 eV, smaller than their binary-blend counterparts.

The external quantum efficiency (EQE) spectra of the binary and ternary blends are shown in Figure 1F,G. The binary blends based on PM6: ITIC-Th and PM6: IT-4F both exhibit narrow photo-response from 300 to 850 nm, which resembles their absorption spectra. As a comparison, the EQE based on D:A blends incorporating Y6

TABLE 1 Photovoltaic parameters of OPV devices based on PM6:Y6, PM6:IT-4F, PM6:Y6:IT-4F, PM6:ITIC-Th, and PM6:Y6:ITIC-Th, with the structure of ITO/PEDOT: PSS/active layer/PNDIT-F3N/Ag, under simulated AM 1.5G irradiation at 100 mW cm^{-2}

Active layer	Weight ratio	V_{OC}[a] (V)	J_{SC}[a] (mA cm^{-2})	calc. J_{SC}[b] (mA cm^{-2})	FF[a] (%)	PCE[a] (%)
PM6:Y6	1:1.2	0.84 (0.84 ± 0.01)	25.5 (25.2 ± 0.3)	25.2	77.4 (76.8 ± 0.8)	16.7 (16.4 ± 0.2)
PM6:Y6:IT-4F	1:1.12:0.08	0.85 (0.84 ± 0.01)	26.0 (25.6 ± 0.3)	25.7	77.4 (77.0 ± 0.5)	17.0 (16.6 ± 0.3)
PM6:Y6:IT-4F	1:1.05:0.15	0.85 (0.85 ± 0.01)	26.0 (25.7 ± 0.3)	25.7	74.8 (74.6 ± 0.5)	16.5 (16.2 ± 0.2)
PM6:IT-4F	1:1.2	0.88 (0.88 ± 0.01)	18.6 (18.4 ± 0.2)	17.7	73.3 (73.0 ± 0.9)	12.0 (11.8 ± 0.2)
PM6:Y6:ITIC-Th	1:1.12:0.08	0.86 (0.85 ± 0.01)	25.6 (25.3 ± 0.4)	25.3	78.2 (77.8 ± 0.9)	17.2 (16.8 ± 0.3)
PM6:Y6:ITIC-Th	1:1.05:0.15	0.87 (0.87 ± 0.01)	25.7 (25.3 ± 0.3)	25.3	76.0 (75.7 ± 1.0)	17.0 (16.6 ± 0.2)
PM6:ITIC-Th	1:1.2	0.98 (0.98 ± 0.01)	16.0 (15.8 ± 0.3)	15.4	69.5 (69.0 ± 0.6)	10.9 (10.5 ± 0.2)

[a]Values for the highest-PCE device, with average values obtained from 20 devices listed in parentheses.
[b]J_{SC} value from the integration of the EQE spectra.

TABLE 2 Charge mobilities and GISAXS fitted data of PM6: Y6, PM6:Y6: IT-4F (1:1.12:0.08), PM6: IT-4F, and PM6:Y6: ITIC-Th (1:1.12:0.08), PM6: ITIC-Th blends

Samples	μ_h (cm^2 V^{-1} $second^{-1}$)	μ_e (cm^2 V^{-1} $second^{-1}$)	μ_h/μ_e	Intermixing domain size (nm)	Acceptor domain size (nm)
PM6:Y6	6.72×10^{-4}	3.96×10^{-4}	1.70	51.3	24.4
PM6:Y6:IT-4F	7.46×10^{-4}	4.41×10^{-4}	1.69	40.3	22.6
PM6:IT-4F	6.03×10^{-4}	3.35×10^{-4}	1.80	67.1	17.9
PM6:Y6:ITIC-Th	6.96×10^{-4}	4.54×10^{-4}	1.53	68.9	28.9
PM6:ITIC-Th	5.89×10^{-4}	3.23×10^{-4}	1.82	80.2	49.3

exhibits photo-response extending to 950 nm. The addition of IT-4F and ITIC-Th flattens the EQE spectra by filling the small valley in the range of approximately 650 to 830 nm. According to the EQE spectra, the respective integrated J_{SC}S of devices based on the PM6:Y6, PM6:Y6: IT-4F (1:1.12:0.08), PM6:Y6:IT-4F (1:1.15:0.05), PM6: IT-4F, PM6: Y6: ITIC-Th (1:1.12:0.08), PM6:Y6: ITIC-Th (1:1.15:0.05), PM6: ITIC-Th blends are 25.2, 25.7, 25.7, 17.7, 25.3, 25.3, and 15.4 mA cm^{-2}, which agree well with the J_{SC} value from the J-V curve (within 5% error).

The photocurrent density (J_{ph}) vs the effective voltage (V_{eff}) is measured to quantify the effect of IT-4F and ITIC-Th in the charge generation and extraction properties (Figure 1H,I and Table S1).[69] At a high V_{eff} of 3 V, J_{ph} is assumed to become fully saturated, being independent of voltage and temperature. The saturated photocurrent density (named J_{sat}) is given by the equation of $J_{sat} = qG_{max}L$, where q is the electric charge, L refers to the thickness of the active layer, and G_{max} represents the maximum generation rate of excitons in OPVs, which is in principle dominated by absorption. The optimized PM6: Y6, PM6: Y6: IT-4F (1:1.12:0.08) and PM6: Y6: ITIC-Th (1:1.12:0.08) present J_{sat}s of 27.2, 27.6, and 27.0 mA cm^{-2}, significantly higher than that of the PM6: IT-4F (20.4 mA cm^{-2}) and PM6: ITIC-Th (18.0 mA cm^{-2}), due to the strong panchromatic absorption from 300 to 1000 nm of Y6. The exciton dissociation efficiency (η_{diss}) and charge collection efficiency (η_{coll}) are calculated under the short circuit and maximum power output conditions, according to the equations of $\eta_{diss} = J_{SC}/J_{sat}$ and $\eta_{coll} = J_{max}/J_{sat}$, respectively. Compared with the PM6: Y6 control, the addition of IT-4F not only slightly increases the J_{sat}, but also elevates η_{diss} from 93.8% to 94.2% and η_{coll} from 85.3% to 86.6%. Besides, although the addition of ITIC-Th has negligible contribution to J_{sat}, it effectively enhances η_{diss} from 93.8% to 94.8% and η_{coll} from 85.3% to 87.4%.

Charge mobility is also fitted from the dark current density-voltage curves using the space-charge-limited current (SCLC) model (Figure S2, Table 2, and Table S2). Electron-only devices employ the architecture of ITO/ZnO/active layer/PNDIT-F3N/Ag, while hole-only devices use the ITO/MoO_x/active layers/MoO_x/Ag. As for pure acceptor film, the pristine electron mobility (μ_e) declines from 6.21×10^{-4} cm^2 V^{-1} $second^{-1}$ for Y6, 5.75×10^{-4} cm^2 V^{-1} $second^{-1}$ for IT-4F, to 5.05×10^{-4} cm^2 V^{-1} $second^{-1}$ for ITIC-Th. This order of magnitude illustrates that all these nonfullerene

acceptors have strong electron transport ability, and Y6 is the best. For the binary blends, the μ_e of PM6: Y6, PM6: IT-4F, PM6: ITIC-Th is 3.96×10^{-4}, 3.35×10^{-4}, and 3.23×10^{-4} cm^2 V^{-1} $second^{-1}$, which resemble the trend of the pure acceptor films, and their hole mobility (μ_h) of the corresponding blend films are 6.72×10^{-4}, 6.03×10^{-4} and 5.89×10^{-4} cm^2 V^{-1} $second^{-1}$. The higher and more balanced charge transport ($\mu_h/\mu_e = 1.70$) in PM6: Y6 blend contributed to the high FF of 77.4%, in comparison with 73.7% for PM6: IT-4F and 69.5% for PM6: ITIC-Th. The PM6:Y6: IT-4F (1:1.12:0.08) blend exhibits μ_h of 7.46×10^{-4} and μ_e of 4.41×10^{-4} cm^2 V^{-1} $second^{-1}$ with μ_h/μ_e of 1.69, while the PM6:Y6: ITIC-Th (1:1.12:0.08) blend exhibits μ_h of 6.96×10^{-4} and μ_e of 4.54×10^{-4} cm^2 V^{-1} $second^{-1}$with μ_h/μ_e of 1.53. Compared with the PM6: IT-4F and PM6: ITIC-Th binary devices, the optimal PM6:Y6: IT-4F and PM6:Y6: ITIC-Th systems exhibited the higher and more balanced mobility, according to their higher charge collection efficiencies of 86.6% and 87.4%, and higher FFs of 77.4% and 78.2%.

To decipher the role of IT-4F and ITIC-Th, the PL spectra of Y6, IT-4F, and ITIC-Th pure films, and Y6: IT-4F and Y6: ITIC-Th blend films (excited at 710 nm) are further measured and plotted in Figure 2. The PL spectra of IT-4F and ITIC-Th, peaking at 808 and 773 nm, strongly overlaps the absorption of Y6 and affords the possibility of energy transfer from IT-4F/ITIC-Th to Y6. The PL intensity of IT-4F pristine film is approximately as much as thrice that of ITIC-Th pristine film. In the Y6: IT-4F blend film, the emission of IT-4F is entirely quenched by Y6 while that of Y6 shows some enhancement, indicating effective energy transfer from IT-4F to Y6, which is in accordance with the slight J_{sat} increase from 27.2 (PM6: Y6) to 27.6 mA cm^{-2} (PM6:Y6: IT-4F). By comparison, the emission of ITIC-Th is also effectively quenched while that of Y6 shows almost negligible enhancement in Y6: ITIC-Th blend, in line with the similar J_{sat} of PM6:Y6: ITIC-Th and PM6: Y6 systems.

Atomic force microscope (AFM) is one of the most widely used tools for surface morphology characterization in the OPV field. It provides the basic information of surface morphology, mainly the surface topography with high spatial resolution within 10 nm. The AFM Height images of binary blends and ternary blends show smooth and uniform surface morphology, which guarantee their good contact with the PNDIT-F3N interlayer (Figures S3 and S4). With the increased ratio of IT-4F, the root mean square roughness (R_q) increased from 1.03 nm for PM6: Y6, 1.40 nm for PM6: Y6: IT-4F, and 2.41 nm for PM6: IT-4F. Likewise, with the increased ratio of ITIC-Th, RMS increased from 1.03 nm for PM6: Y6, 1.22 nm for PM6:Y6: ITIC-Th, and 1.79 nm for PM6: ITIC-Th. AFM can only probe the surface information of the active layer, while the inward donor/acceptor configuration is pivotal for device performance. Grazing incidence wide-angle X-ray scattering (GIWAXS) is therefore adopted to investigate crystalline structures on the molecular scale, including information of the distance of the lamellar layers, π-π stacking, and crystalline coherence length (CCL).[70-72] The 2D diffraction patterns and 1D line-cuts are depicted in Figures 3A-G, S5, and S6. The PM6 neat film exhibits a π-π peak at $q_z \approx 1.70$ $Å^{-1}$ ($d \approx 3.70$ Å) along the out-of-plane (OOP) direction and bimodal lamellar peaks in both in-plane (IP) and OOP directions at $q_r \approx 0.281$ $Å^{-1}$ ($d \approx 22.4$ Å) and $q_z \approx 0.303$ $Å^{-1}$ ($d \approx 20.7$ Å). The Y6 neat film exhibits a strong π-π stacking peak at $q_z \approx 1.76$ $Å^{-1}$ ($d \approx 3.57$ Å), indicating a preferential face-on orientation of Y6. It is noteworthy that the co-existence of two diffraction peaks at $q_r \approx 0.285$ $Å^{-1}$ ($d \approx 22.0$ Å) and $q_r \approx 0.420$ $Å^{-1}$ ($d \approx 15.0$ Å) in Y6 film drops a hint of the concomitance of two distinct structure

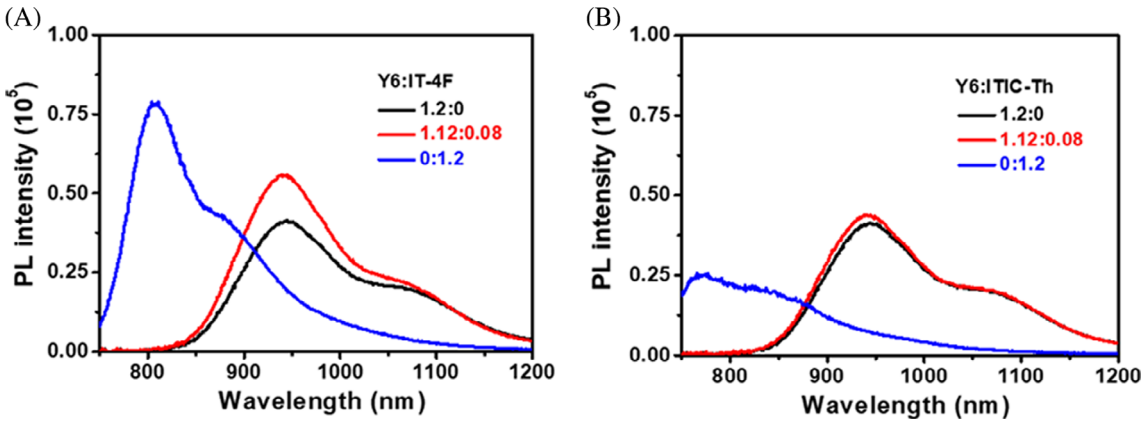

FIGURE 2 A, PL spectra of Y6 and IT-4F pure films and Y6: IT-4F blend film; and B, PL spectra of Y6 and ITIC-Th pure films and Y6: ITIC-Th blend film. (excited at 710 nm)

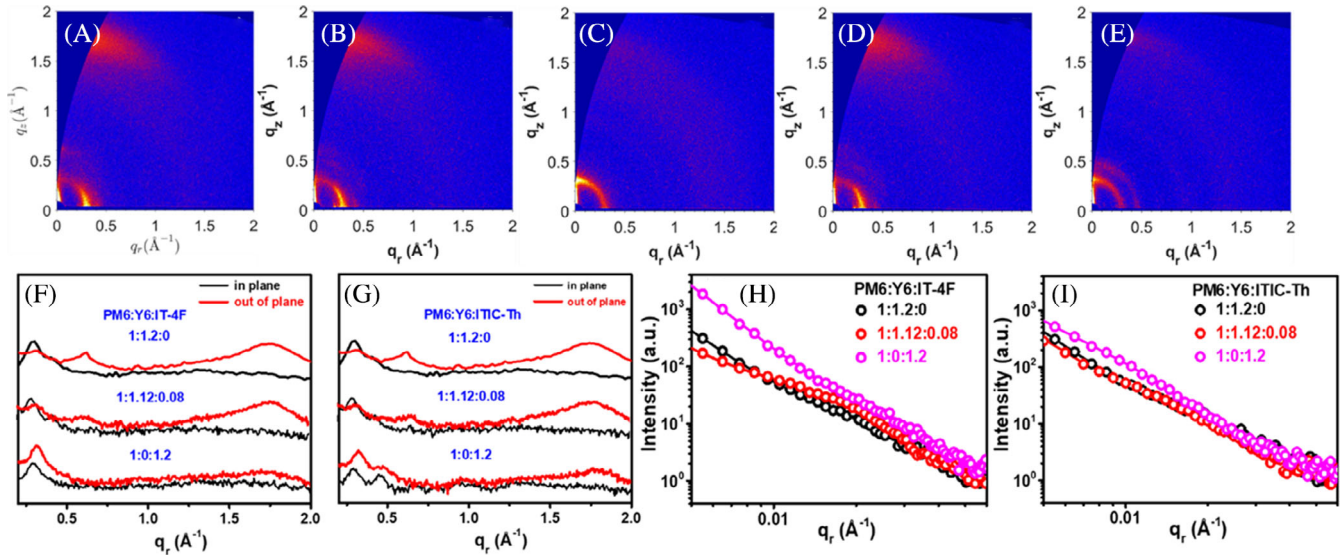

FIGURE 3 GIWAXS two-dimensional diffraction patterns of A, PM6: Y6 blend; B, PM6:Y6: IT-4F (1:1.12:0.08) blend; C, PM6: IT-4F blend; D, PM6:Y6: ITIC-Th (1:1.12:0.08) blend and E, PM6: ITIC-Th blend. F, The out-of-plane (red line) and in-plane (black line) line-cut profiles of PM6: Y6, PM6:Y6: IT-4F (1:1.12:0.08), and PM6: IT-4F blends. G, The out-of-plane (red line) and in-plane (black line) line-cut profiles of PM6: Y6, PM6:Y6: IT-4F (1:1.12:0.08), and PM6: IT-4F blends. H, GISAXS intensity profiles with best fittings along the in-plane direction of PM6: Y6, PM6:Y6: IT-4F (1:1.12:0.08), and PM6: IT-4F blends. I, GISAXS intensity profiles with best fittings along the in-plane direction of PM6: Y6, PM6:Y6: ITIC-Th (1:1.12:0.08), and PM6: ITIC-Th blends

orders. Since one of the IP diffraction peaks is assigned to the lamellar peak, the other presumably originate from the backbone ordering shaped by the π-π stacking of end groups.[38] This unusual phenomenon is also observed in the pristine film of ITIC-Th, which mainly exhibited two diffraction peaks at $q_r \approx 0.352$ Å^{-}1 and $q_r \approx 0.466$ Å^{-1}, and π-π peak at $q_z \approx 1.77$ Å^{-1}. The IT-4F pristine film exhibited lamellar peaks at $q_r \approx 0.354$ Å^{-}1, with an extremely weak π-π peak. Among all the blend films, the PM6: Y6 blend takes on preferential face-on packing by exhibiting a strong OOP (010) peaks at $q_z \approx 1.73$ Å^{-1} ($d \approx 3.63$ Å) and bimodal (100) peaks at $q_r \approx 0.293$ Å^{-1} ($d \approx 21.4$ Å) and $q_z \approx 0.296$ Å^{-1} ($d \approx 21.2$ Å). The PM6: IT-4F blend presented bimodal lamellar peaks at $q_r \approx 0.295$ Å^{-1} ($d \approx 21.3$ Å) and $q_z \approx 0.315$ Å^{-1} ($d \approx 19.9$ Å), and π-π peak at $q_z \approx 1.68$ Å^{-1} ($d \approx 3.74$ Å), indicating its relatively incompact π-π stacking. Interestingly, as Table S3 shows, the slight doping of IT-4F into PM6: Y6 blend increased the CCL of the OOP π-π peak of PM6: Y6 blend from 23.3 to 25.2 Å. (CCL is calculated based on the equation: CCL = 1.8 × π/FWHM, where the FWHM is short for the full width at half-maximum.) The PM6: ITIC-Th blend presented bimodal lamellar peaks at $q_r \approx 0.291$ Å^{-1} ($d \approx 21.6$ Å) and $q_z \approx 0.320$ Å^{-1} ($d \approx 19.6$ Å), and π-π peak at $q_z \approx 1.78$ Å^{-1} ($d \approx 3.53$ Å), indicating its tighter π-π stacking than PM6: Y6 blend. The addition of ITIC-Th into PM6: Y6 blend also increased the CCL of the OOP π-π peak from 23.3 to 24.1 Å, and decreased the π-π d-spacing from 3.63 ($q_z \approx 1.73$ Å^{-1}) to 3.59 Å ($q_z \approx 1.75$ Å^{-1}).

Grazing incidence small-angle X-ray scattering (GISAXS) is supplemented to investigate nanoscale phase separation in thin films. Figure 3H,I presented GISAXS intensity profiles with best fittings along the in-plane direction of PM6: Y6, PM6:Y6: ITIC-Th, and PM6: ITIC-Th blends. The data were fitted with fractal-like network models and Debye-Anderson-Brumberger (DAB) models, to account for the scattering contribution from acceptor domains and the intermixing amorphous phase, respectively (Table 2). The pure acceptor domain size gradually decreased from 24.4 nm for PM6: Y6, to 22.6 nm for PM6: Y6: IT-4F (1:1.12:0.08) and 17.9 nm for PM6: IT-4F, and increased monotonically from PM6: Y6 (24.4 nm), PM6: Y6: ITIC-Th (28.9 nm) to PM6: ITIC-Th with an excessively large acceptor domain size of 49.3 nm. Comparing PM6: Y6 and PM6:Y6: ITIC-Th blends, the increased acceptor domain size in the latter blend potentially favors electron transport, and can partially account for the increased electron mobilities from 3.96×10^{-4} to 4.54×10^{-4} cm^2 V^{-1} second^{-1}. Besides, it is understandable that PM6:Y6: IT-4F exhibited the higher electron mobilities than the PM6: Y6 control, which is attributed to the increased CCL of oop π-π peak and the decreased electron energy disorder.[73-75] All the blend films exhibited reasonable phase segregation scales with acceptor domain size around 20 nm, except for the PM6: ITIC-Th blend with an acceptor domain size of approximately 49.3 nm. The excessively large phase separation in PM6: ITIC-Th devices is unfavorable for charge separation,

and accounts for its lowest exciton dissociation efficiency (88.9%).

3 | CONCLUSION

To summarize, we improved the device processing and performance of PM6:Y6: IT-4F based OPVs, and further incorporated ITIC-Th with higher LUMO into the PM6: Y6 blend. The PM6:Y6: ITIC-Th device afforded a PCE of 17.2%, which outcompeted PM6: Y6 control device and became one of the highest PCE for OPVs. PM6:Y6 system demonstrated small E_{loss} but low voltage; by contrast, PM6:ITIC-Th system demonstrated high voltage but large E_{loss}. The resulting PM6:Y6: ITIC-Th OSCs interestingly demonstrated the lowest E_{loss} along with over 17% PCE. The incorporation of ITIC-Th and IT-4F can balance the charge mobilities, and thereby retain and improve FF. Increased crystalline coherence length and smaller d-spacing of π-π peaks are observed with the third component incorporation, indicating enhanced crystallinity and thus improved active-layer morphology. It is also found that the energy transfer from IT-4F to Y6 is more evident than that from ITIC-Th to Y6. Our findings demonstrate the practicability of "new use for an old drug" strategy to pursue breakthroughs of OPVs.[75]

ACKNOWLEDGMENTS

Cenqi Yan and Ruijie Ma contributed equally to this work. Gang Li thanks the support from the Research Grants Council of Hong Kong (15218517, C5037-18G), Shenzhen Science and Technology Innovation Commission (JCYJ20170413154602102), the funding for Project of Strategic Importance (1-ZE29), Sir Sze-yuen Chung Endowed Professorship fund provided by the Hong Kong Polytechnic University, and National Natural Science Foundation of China (51961165102). Gang Li and Cenqi Yan thank the Hong Kong Polytechnic University for Postdoctoral Fellowships Scheme (YW3Y). He Yan thanks the support from the National Key Research and Development Program of China (2019YFA0705900) funded by MOST, the Research Grants Council of Hong Kong (R6021-18, 16305915, 16322416, 606012, and 16303917), the Shenzhen Technology and Innovation Commission (JCYJ20170413173814007 and JCYJ20170818113905024), and Hong Kong Innovation and Technology Commission for the support through projects ITC-CNERC14SC01 and ITS/471/18). Ruijie Ma acknowledges the support from Hong Kong PhD Fellowship Scheme (PF17-03929). Xinhui Lu thanks the Research Grant Council of Hong Kong (14314216).

CONFLICT OF INTEREST

The authors declare no conflict of interest.

ORCID

Ruijie Ma https://orcid.org/0000-0002-7227-5164
Gang Li https://orcid.org/0000-0001-8399-7771

REFERENCES

1. Yan C, Barlow S, Wang Z, et al. Non-fullerene acceptors for organic solar cells. *Nat Rev Mater*. 2018;3(3):18003.
2. Li G, Chang WH, Yang Y. Low-bandgap conjugated polymers enabling solution-processable tandem solar cells. *Nat Rev Mater*. 2017;2(8):17043.
3. Li Y. Molecular design of photovoltaic materials for polymer solar cells: toward suitable electronic energy levels and broad absorption. *Acc Chem Res*. 2012;45(5):723-733.
4. Li G, Zhu R, Yang Y. Polymer solar cells. *Nat Photonics*. 2012;6(3):153-161.
5. Xue QF, Xia RX, Brabec CJ, Yip HL. Recent advances in semi-transparent polymer and perovskite solar cells for power generating window applications. *Energ Environ Sci*. 2018;11(7):1688-1709.
6. Hou J, Inganas O, Friend RH, Gao F. Organic solar cells based on non-fullerene acceptors. *Nat Mater*. 2018;17(2):119-128.
7. Cheng P, Li G, Zhan XW, Yang Y. Next-generation organic photovoltaics based on non-fullerene acceptors. *Nat Photonics*. 2018;12(3):131-142.
8. Nielsen CB, Holliday S, Chen HY, Cryer SJ, McCulloch I. Non-fullerene electron acceptors for use in organic solar cells. *Acc Chem Res*. 2015;48(11):2803-2812.
9. Fukuda K, Yu K, Someya T. The future of flexible organic solar cells. *Adv Energy Mater*. 2020;10:2000765.
10. Mainville M, Leclerc M. Recent Progress on indoor organic photovoltaics: from molecular design to production scale. *ACS Energy Lett*. 2020;5(4):1186-1197.
11. Kumar A, Devine R, Mayberry C, Lei B, Li G, Yang Y. Origin of Radiation-Induced Degradation in Polymer Solar Cells. *Adv Mater*. 2010;20(16):2729–2736. http://dx.doi.org/10.1002/adfm.201000374.
12. Wang JY, Zhan XW. Rylene Diimide electron acceptors for organic solar cells. *Trend Chem*. 2019;1(9):869-881.
13. Liu DL, Zhang Y, Li G. Nanomorphology in A-D-A type small molecular acceptors-based bulk heterojunction polymer solar cells. *J Energy Chem*. 2019;35:104-123.
14. Huo Y, Zhang HL, Zhan XW. Nonfullerene all-small-molecule organic solar cells. *ACS Energy Lett*. 2019;4(6):1241-1250.
15. Liu QS, Jiang YF, Jin K, et al. 18% efficiency organic solar cells. *Sci Bull*. 2020;65(4):272-275.
16. Meng L, Zhang Y, Wan X, et al. Organic and solution-processed tandem solar cells with 17.3% efficiency. *Science*. 2018;361(6407):1094-1098.
17. Cui Y, Yao H, Zhang J, et al. Single-junction organic photovoltaic cells with approaching 18% efficiency. *Adv Mater*. 2020;32(19):1908205.
18. Sun H, Tang Y, Koh CW, et al. High-performance all-polymer solar cells enabled by an n-type polymer based on a fluorinated imide-functionalized Arene. *Adv Mater*. 2019;31(15):1807220.

19. Sun H, Guo X, Facchetti A. High-performance n-type polymer semiconductors: applications, recent development, and challenges. *Chem*. 2020;6(6):1310-1326.
20. Sun H, Liu B, Yu J, et al. Reducing energy loss via tuning energy levels of polymer acceptors for efficient all-polymer solar cells. *Sci China Chem*. 2020. https://doi.org/10.1007/s11426-020-9826-4.
21. Naveed HB, Zhou K, Ma W. Interfacial and bulk nanostructures control loss of charges in organic solar cells. *Acc Chem Res*. 2019;52(10):2904-2915.
22. An QS, Zhang FJ, Zhang J, Tang WH, Deng ZB, Hu B. Versatile ternary organic solar cells: a critical review. *Energ Environ Sci*. 2016;9(2):281-322.
23. Lu LY, Kelly MA, You W, Yu LP. Status and prospects for ternary organic photovoltaics. *Nat Photonics*. 2015;9(8):491-500.
24. Liu T, Luo ZH, Chen YZ, et al. A nonfullerene acceptor with a 1000 nm absorption edge enables ternary organic solar cells with improved optical and morphological properties and efficiencies over 15%. *Energ Environ Sci*. 2019;12(8):2529-2536.
25. Fan QP, Liu T, Zhang M, et al. Weak makes it powerful: the role of cognate small molecules as an alloy donor in 2D/1A ternary fullerene solar cells for finely tuned hierarchical morphology in thick active layers. *Small Methods*. 2020;4:1900766.
26. Liu T, Luo Z, Fan Q, et al. Use of two structurally similar small molecular acceptors enabling ternary organic solar cells with high efficiencies and fill factors. *Energ Environ Sci*. 2018;11(11):3275-3282.
27. Liu T, Xue XN, Huo LJ, et al. Highly efficient parallel-like ternary organic solar cells. *Chem Mater*. 2017;29(7):2914-2920.
28. Yang Y, Chen W, Dou LT, et al. High-performance multiple-donor bulk heterojunction solar cells. *Nat Photonics*. 2015;9(3):190-198.
29. Cheng P, Yan C, Lau T-K, Mai J, Lu X, Zhan X. Molecular lock: a versatile key to enhance efficiency and stability of organic solar cells. *Adv Mater*. 2016;28(28):5822-5829.
30. Cheng P, Wang R, Zhu JS, et al. Ternary system with controlled structure: a new strategy toward efficient organic photovoltaics. *Adv Mater*. 2018;30(8):1705243.
31. Wang W, Yan CQ, Lau TK, et al. Fused Hexacyclic nonfullerene acceptor with strong near-infrared absorption for semitransparent organic solar cells with 9.77% efficiency. *Adv Mater*. 2017;29(31):1701308.
32. Zhang J, Yan C, Wang W, et al. Panchromatic ternary photovoltaic cells using a nonfullerene acceptor synthesized using C–H functionalization. *Chem Mater*. 2018;30:309-−313.
33. Liu D, Zhang Y, Zhan L, et al. Design of wide-bandgap polymers with deeper ionization potential enables efficient ternary non-fullerene polymer solar cells with 13% efficiency. *J Mater Chem A*. 2019;7(23):14153-14162.
34. Zhang Y, Liu D, Fong PW, Li G. Investigation of low-bandgap nonfullerene acceptor-based polymer solar cells with very low photovoltage loss. *J Photon Energy*. 2019;9(4):045502.
35. Zhang Y, Liu DL, Lau TK, et al. A novel wide-bandgap polymer with deep ionization potential enables exceeding 16% efficiency in ternary nonfullerene polymer solar cells. *Adv Funct Mater*. 2020;30(27):1910466.
36. Feng L, Yuan J, Zhang Z, et al. Thieno[3,2-b]pyrrolo-fused Pentacyclic Benzotriazole-based acceptor for efficient organic photovoltaics. *ACS Appl Mater Interfaces*. 2017;9(37):31985-31992.
37. Yuan J, Huang T, Cheng P, et al. Enabling low voltage losses and high photocurrent in fullerene-free organic photovoltaics. *Nat Commun*. 2019;10(1):570.
38. Yuan J, Zhang Y, Zhou L, et al. Single-junction organic solar cell with over 15% efficiency using fused-ring acceptor with electron-deficient Core. *Joule*. 2019;3(4):1140-1151.
39. Liu S, Yuan J, Deng WY, et al. High-efficiency organic solar cells with low non-radiative recombination loss and low energetic disorder. *Nat Photon*. 2020;14:300-305.
40. Wei Q, Liu W, Leclerc M, Yuan J, Chen H, Zou Y. A-DA′D-A non-fullerene acceptors for high-performance organic solar cells. *Sci China Chem*. 2020;63:1352-1366. https://doi.org/10.1007/s11426-11020-19799-11424.
41. Fan Q, Wang Y, Zhang M, et al. High-performance as-cast nonfullerene polymer solar cells with thicker active layer and large area exceeding 11% power conversion efficiency. *Adv Mater*. 2018;30(6):1704546.
42. Zhang M, Guo X, Ma W, Ade H, Hou J. A large-bandgap conjugated polymer for versatile photovoltaic applications with high performance. *Adv Mater*. 2015;27(31):4655-4660.
43. Luo ZH, Ma RJ, Liu T, et al. Fine-tuning energy levels via asymmetric end groups enables polymer solar cells with efficiencies over 17%. *Joule*. 2020;4(6):1236-1247.
44. Chen HY, Hu DQ, Yang QG, et al. All-small-molecule organic solar cells with an ordered liquid crystalline donor. *Joule*. 2019;3(12):3034-3047.
45. Sun HL, Liu T, Yu JW, et al. A monothiophene unit incorporating both fluoro and ester substitution enabling high-performance donor polymers for non-fullerene solar cells with 16.4% efficiency. *Energ Environ Sci*. 2019;12(11):3328-3337.
46. Zhu L, Zhang M, Zhou GQ, et al. Efficient organic solar cell with 16.88% efficiency enabled by refined acceptor crystallization and morphology with improved charge transfer and transport properties. *Adv Energy Mater*. 2020;10:1904234.
47. Xu X, Feng K, Bi Z, Ma W, Zhang G, Peng Q. Single-junction polymer solar cells with 16.35% efficiency enabled by a platinum(II) complexation strategy. *Adv Mater*. 2019;31(29):1901872.
48. Ma R, Liu T, Luo Z, et al. Improving open-circuit voltage by a chlorinated polymer donor endows binary organic solar cells efficiencies over 17%. *Sci China Chem*. 2020;63(3):325-330.
49. An QS, Wang J, Gao W, et al. Alloy-like ternary polymer solar cells with over 17.2% efficiency. *Sci Bull*. 2020;65(7):538-545.
50. Zhan L, Li S, Lau T-K, et al. Over 17% efficiency ternary organic solar cells enabled by two non-fullerene acceptors working in alloy-like model. *Energ Environ Sci*. 2020;13:635-645.
51. Liu T, Zhang YD, Shao YM, et al. Asymmetric acceptors with fluorine and chlorine substitution for organic solar cells toward 16.83% efficiency. *Adv Funct Mater*. 2020;30(24):2000456.
52. Zeng M, Wang X, Ma R, et al. Dopamine Semiquinone radical doped PEDOT:PSS: enhanced conductivity, work function and performance in organic solar cells. *Adv Energy Mater*. 2020;10:2000743.
53. Luo Z, Sun R, Zhong C, et al. Altering alkyl-chains branching positions for boosting the performance of small-molecule acceptors for highly efficient nonfullerene organic solar cells. *Sci China Chem*. 2020;63(3):361-369.
54. Liu T, Ma R, Luo Z, et al. Concurrent improvement in JSC and VOC in high-efficiency ternary organic solar cells enabled by a

red-absorbing small-molecule acceptor with a high LUMO level. *Energ Environ Sci*. 2020;13(7):2115-2123.
55. Hu DQ, Yang QG, Chen HY, et al. 15.34% efficiency all-small-molecule organic solar cells with an improved fill factor enabled by a fullerene additive. *Energ Environ Sci*. 2020;13(7):2134-2141.
56. Tang H, Chen H, Yan C, et al. Delicate morphology control triggers 14.7% efficiency all-small-molecule organic solar cells. *Adv Energy Mater*. 2020;10(27):2001076.
57. Tang H, Xu T, Yan C, et al. Donor derivative incorporation: An effective strategy toward high performance all-small-molecule ternary organic solar cells. *Adv Sci*. 2019;6:1901613.
58. Fu JH, Chen SS, Yang K, et al. A "sigma-Hole"-containing volatile solid additive enabling 16.5% efficiency organic solar cells. *Iscience*. 2020;23(3):100965.
59. Wu Y, Zheng Y, Yang H, et al. Rationally pairing photoactive materials for high-performance polymer solar cells with efficiency of 16.53%. *Sci China Chem*. 2020;63(2):265-271.
60. Fan B, Zeng Z, Zhong W, et al. Optimizing microstructure morphology and reducing electronic losses in 1 cm2 polymer solar cells to achieve efficiency over 15%. *ACS Energy Lett.* 2019;4(10):2466-2472.
61. Fan BB, Zhang DF, Li MJ, et al. Achieving over 16% efficiency for single-junction organic solar cells. *Sci China Chem*. 2019;62(6):746-752.
62. Xiong J, Jin K, Jiang YF, et al. Thiolactone copolymer donor gifts organic solar cells a 16.72% efficiency. *Sci Bull*. 2019;64(21):1573-1576.
63. Wang T, Qin JQ, Xiao Z, et al. A 2.16 eV bandgap polymer donor gives 16% power conversion efficiency. *Sci Bull.* 2020;65(3):179-181.
64. Yan T, Song W, Huang J, Peng R, Huang L, Ge Z. 16.67% rigid and 14.06% flexible organic solar cells enabled by ternary heterojunction strategy. *Adv Mater*. 2019;31(39):1902210.
65. An QS, Ma XL, Gao JH, Zhang FJ. Solvent additive-free ternary polymer solar cells with 16.27% efficiency. *Sci Bull*. 2019;64(8):504-506.
66. Zhao WC, Li SS, Yao HF, et al. Molecular optimization enables over 13% efficiency in organic solar cells. *J Am Chem Soc*. 2017;139(21):7148-7151.
67. Lin Y, Zhao F, He Q, et al. High-performance electron acceptor with Thienyl side chains for organic photovoltaics. *J Am Chem Soc*. 2016;138(14):4955-4961.
68. Wu Z, Sun C, Dong S, et al. N-type water/alcohol-soluble naphthalene diimide-based conjugated polymers for high-performance polymer solar cells. *J Am Chem Soc*. 2016;138(6):2004-2013.
69. Mihailetchi VD, Koster LJA, Hummelen JC, Blom PWM. Photocurrent generation in polymer-fullerene bulk heterojunctions. *Phys Rev Lett*. 2004;93(21):216601.
70. Zhao FW, Wang CR, Zhan XW. Morphology control in organic solar cells. *Adv Energy Mater*. 2018;8:1703147.
71. Mai JQ, Xiao YQ, Zhou GD, et al. Hidden structure ordering along backbone of fused-ring electron acceptors enhanced by ternary bulk heterojunction. *Adv Mater*. 2018;30(34):1802888.
72. Mai JQ, Lau TK, Li J, et al. Understanding morphology compatibility for high-performance ternary organic solar cells. *Chem Mater*. 2016;28(17):6186-6195.
73. Yin H, Chiu KL, Bi PQ, et al. Enhanced electron transport and heat transfer boost light stability of ternary organic photovoltaic cells incorporating non-fullerene small molecule and polymer acceptors. *Adv Electron Mater*. 2019;5:1900497.
74. Ma R, Liu T, Luo Z, et al. Adding a third component with reduced miscibility and higher LUMO level enables efficient ternary organic solar cells. *ACS Energy Lett*. 2020;5:2711-2720.
75. Tang H, Yan C, Karuthedath S, et al. Deciphering the role of fluorination: morphological manipulation prompts charge separation and reduces carrier recombination in all-small-molecule photovoltaics. *Sol RRL*. 2020;4:1900528.

SUPPORTING INFORMATION

Additional supporting information may be found online in the Supporting Information section at the end of this article.

How to cite this article: Yan C, Ma R, Cai G, et al. Reducing V_{OC} loss via structure compatible and high lowest unoccupied molecular orbital nonfullerene acceptors for over 17%-efficiency ternary organic photovoltaics. *EcoMat*. 2020;2:e12061. https://doi.org/10.1002/eom2.12061